

# A peculiar interacting Be star binary in the Small Magellanic Cloud <sup>☆</sup>

Ronald E. Mennickent<sup>a</sup>, Thomas Rivinius<sup>b</sup>, Lydia Cidale<sup>c,d,e</sup>, Igor Soszyński<sup>f</sup>, J. G. Fernández-Trincado<sup>a,g</sup>

<sup>a</sup>*Departamento de Astronomía, Casilla 160-C, Universidad de Concepción, Chile*

<sup>b</sup>*European Organization for Astronomical Research in the Southern Hemisphere, Casilla 19001, Santiago 19, Chile*

<sup>c</sup>*Facultad de Ciencias Astronómicas y Geofísicas, Universidad de La Plata, Argentina*

<sup>d</sup>*Instituto de Astrofísica de La Plata, CONICET-UNLP, Argentina*

<sup>e</sup>*Instituto de Física y Astronomía, Facultad de Ciencias, Universidad de Valparaíso, Av. Gran Bretaña 1111, Casilla 5030, Valparaíso, Chile*

<sup>f</sup>*Warsaw University Observatory, Al. Ujazdowskie 4, 00-478 Warszawa, Poland*

<sup>g</sup>*Institut Utinam, CNRS UMR6213, Univ. Bourgogne Franche-Comté, OSU THETA, Observatoire de Besançon, BP 1615, 25010 Besançon Cedex, France*

---

## Abstract

We find that the emission line object OGLEJ005039.05-725751.4, a member of the cluster OGLE-CL SMC 64, exhibits a peculiar light curve pattern repeating with a recurrence time of 141.45 days. The light curve resembles periodic outbursts with a duty cycle of 20%. A second long-cycle of 2500 days is also detected in the photometric dataset. Two X-SHOOTER spectra obtained at minimum and maximum reveal a Be star dominating at minimum light resembling the Classical Be star 48 Lib. The larger H $\alpha$  emission, the stronger NaD absorption and the appearance of emission in the infrared Ca II triplet at maximum, might indicate periodic mass transfer in a complex binary system.

*Keywords:* stars:binary, stars: emission line, stars: evolution

---

<sup>☆</sup>Based on the ESO proposal 098.D-0099(A)

*Email address:* `rmennick@udec.cl` (Ronald E. Mennickent)

## 1. Introduction

The object OGLEJ005039.05-725751.4 ( $V = 17.211$  mag,  $\alpha_{2000} = 00:50:39.1630$ ,  $\delta_{2000} = -72:57:51.239$ )<sup>1</sup> is a member of the Small Magellanic Cloud, and it was classified as a Be star candidate, based on optical colors and light curve variability by Mennickent et al. (2002). Later, and consistently with this classification, H $\alpha$  emission was reported in a slitless survey by Martayan, Baade and Fabregat (2010). The object is a member of the cluster OGLE-CL SMC 64 (Bica & Dutra 2000), and possibly is the same object catalogued as 2MASS J00504006-7257492 (SSTISAGEMMA J005040.07-725749.3) with coordinates  $\alpha_{2000} = 00:50:40.067$ ,  $\delta_{2000} = -72:57:49.21$  and labeled as a possible red giant branch star in the SIMBAD database.

The light curve of OGLEJ005039.05-725751.4 shows an extremely rare, strict repeatability of a Be-star outburst like brightening with a period of 141.45 days. In order to investigate the nature of this object we obtained two spectra at maximum and minimum light. The analysis of these spectra and survey light curve is reported in this paper. A finding chart for the star and its surrounding stellar field is shown in Fig. 1.

The paper is organized as follow: in Section 2 we introduce the photometric datasets used in our analysis, details of our spectroscopic observations are given in Section 3, in Section 4 we present our results including the light curve analysis and the study of the spectroscopic data. In Section 5 a discussion is provided along with a possible interpretation for the system and finally our conclusions are given in Section 6.

## 2. Photometric data

The photometric time-series data analyzed in this paper were taken from the OGLE project databases. We included OGLE-II data [20]<sup>2</sup> and OGLE-III/IV data<sup>3</sup>. The OGLE-IV project is described by Udalski, Szymański, & Szymański [21]. The whole dataset consists of 1501  $I$ -band magnitudes and 143  $V$ -band magnitudes taken during a time interval of 17.08 years. A summary of these datasets is given in Table 1.

---

<sup>1</sup><http://simbad.u-strasbg.fr/simbad/>

<sup>2</sup><http://ogledb.astrouw.edu.pl/~ogle/photdb/>

<sup>3</sup> OGLE-III/IV data kindly provided by the OGLE team.

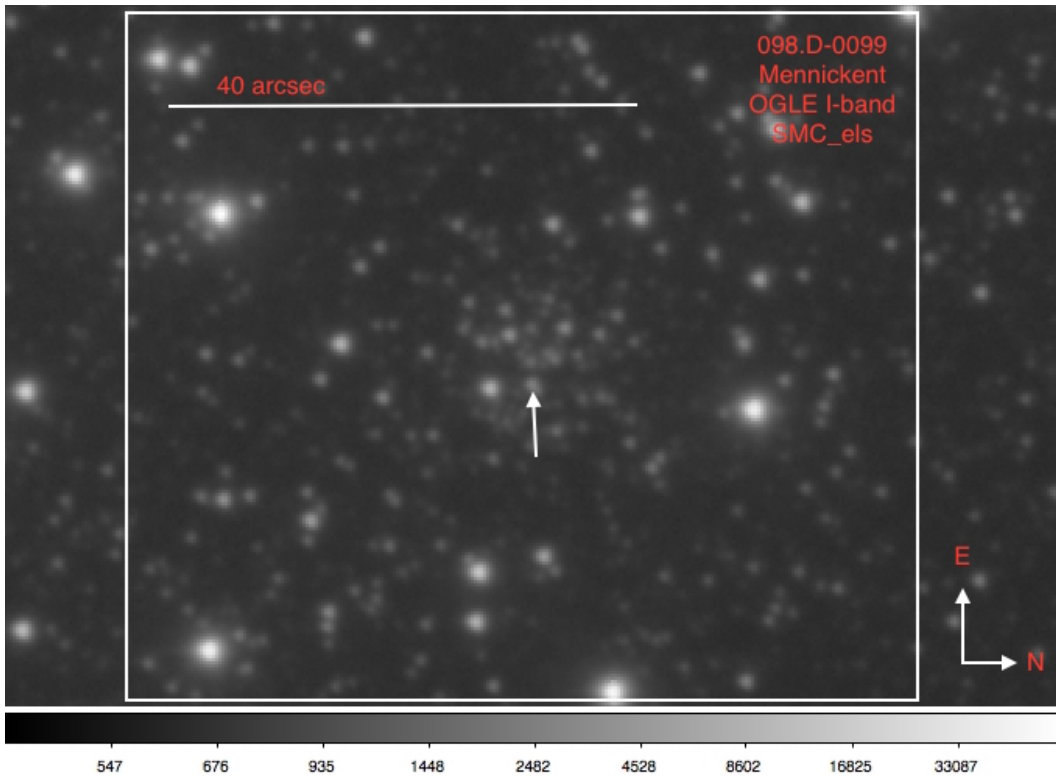


Figure 1: The stellar field around OGLEJ005039.05-725751.4 according to an OGLE *I*-band image. OGLEJ005039.05-725751.4 is shown by the arrow at the center of the image.

Table 1: Summary of survey photometric observations. The number of measurements, starting and ending times for the series and average magnitude and standard deviation (in magnitude) are given. The zero point of HJD is 2 450 000. Single point uncertainties in the *I*-band and *V*-band are between 4 and 6 mmag.

Database	N	$HJD_{start}$	$HJD_{end}$	mag	std.	band
OGLE-II	332	466.5440	1871.7550	16.543	0.126	<i>I</i>
OGLE-III	732	2085.9091	4954.8884	16.864	0.174	<i>I</i>
OGLE-IV	437	5346.9189	6704.5196	16.909	0.143	<i>I</i>
OGLE-II	44	466.5830	1543.6290	17.037	0.056	<i>V</i>
OGLE-III	53	3326.5608	4954.8940	17.053	0.056	<i>V</i>
OGLE-IV	46	5391.9156	6601.5731	17.053	0.061	<i>V</i>

Table 2: Summary of X-SHOOTER spectroscopic observations. The heliocentric Julian day ( $HJD' \equiv HJD - 2\,457\,900$ ) at mid-exposure and wavelength range are given,  $R$  is resolving power and  $S/N$  signal-to-noise ratio measured around 400 and 680 nm.  $\Phi$  refers to the phase to the ephemerides given by Eq. 1.

Night (2017)	$\Delta\lambda$ (nm)	$R$	exptime (s)	$S/N$	HJD'	$\Phi$
2/3-Jun	534–1020	5400	1260	35	07.90506	0.753
2/3-Jun	299–556	7400	1161	55	07.90454	0.753
12/13-Jul	534–1020	5400	1260	10	47.77828	0.035
12/13-Jul	299–556	7400	1161	50	47.77776	0.035

31 We considered to study the spectral energy distribution of this object with  
32 broad-band photometry provided by the VizieR photometric tool <sup>4</sup>. This  
33 on-line tool extracts the magnitudes published in surveys and catalogues,  
34 based in a search performed around a given location, considering a searching  
35 radius. We find that the scatter shown by the fluxes is quite large, more than  
36 expected from the variability of the object, and unfortunately inadequate  
37 for our study. It is possible that the presence of several nearby objects in  
38 the crowded field is the origin of this scatter, considering that automatic  
39 photometric algorithms might fail in such circumstances.

<sup>4</sup><http://vizier.u-strasbg.fr/vizier/sed/doc/>

### 40 **3. Spectroscopic data**

41 We obtained two spectra for OGLEJ005039.05-725751.4 during the nights  
42 of June 2-3 and July 12-13 2017 with the ESO X-SHOOTER spectrograph.  
43 This three-arms echelle spectrograph is located on Unit Telescope 2 (UT2,  
44 Kueyen) of the Very Large Telescope (VLT) at the Paranal Observatory,  
45 Chile, and provides intermediate resolution spectroscopy across a wide wave-  
46 length range, from the ultraviolet (UV) to the near-infrared (NIR). Our ob-  
47 serving setup was optimized to get good recognizing spectra with minimum  
48 exposure time in the UV and optical ranges neglecting the infrared output  
49 and during the minimum (June observations) and maximum (July observa-  
50 tions) of the photometric cycle described in Section 4. Slit widths of 1.0 arcsec  
51 (blue) and 0.9 arcsec (red) were used. The spectra were reduced using the X-  
52 SHOOTER pipeline, including bias removal, wavelength and flux calibration  
53 corrected by atmospheric differential refraction. Due to the crowdedness of  
54 the field, and to avoid including faint nearby stars in the spectrum, the sky  
55 was subtracted only in the visual range. One additional step was to remove  
56 the barycentric earth’s velocity, hence the velocities given here are referred  
57 to the center of mass of the solar system. NIR observations are not consid-  
58 ered in this study because of the extremely low signal-to-noise ratio of the  
59 spectra. Our spectroscopic observations are summarized in Table 2.

### 60 **4. Results**

#### 61 *4.1. Analysis of the light curve*

62 We shifted OGLE-II magnitudes to fit the mean of OGLE-III and OGLE-  
63 IV data. 17.5 years of OGLE-I and V-band photometry show light modu-  
64 lations similar to outbursts recurring with a period of 141.45 days (Fig. 2).  
65 The period was obtained with the PDM task [19] available in the NOAO soft-  
66 ware “Image Reduction and Analysis Facility” (IRAF<sup>5</sup>). These “outbursts”  
67 have a duty cycle of 20% and an amplitude much larger in *I*- than in the  
68 *V*-band; their shapes are almost constant, with a first excursion to a local  
69 maximum, followed by a small brightness decrease and then a second excu-  
70 sion to the maximum occurring around  $I = 16.4$ . The system returns to

---

<sup>5</sup> IRAF is distributed by the National Optical Astronomy Observatory, which is oper-  
ated by the Association of Universities for Research in Astronomy (AURA) under coop-  
erative agreement with the National Science Foundation. <http://iraf.noao.edu>

71 minimum passing again by a dip and secondary peak as revealed in Figs. 2  
 72 and 3. The maxima occur at the same time in both bands, but the minimum  
 73 seems to occur earlier in  $V$ -band than in  $I$ -band (Fig. 4). The  $V - I$  color at  
 74 minimum (+0.12) is compatible with a F1 supergiant but at maximum the  
 75 star is redder;  $V - I = 0.63$  indicates a F5 spectral type (see also Fig. 2).  
 76 In addition to the main light modulation, we find a very long cycle of time  
 77 scale  $T \sim 2500$  days, more evident in the lower envelope of the  $I$ -band light  
 78 curve in the top panel of Fig. 2. We find the following ephemerides for the  
 79 maxima:

$$HJD_{max} = 245\,0587.40 + 141.45 E \quad (1)$$

80 We searched for additional periodicities outside outburst, considering  
 81 data only in the phase range 0.3-0.9 and removing the 141.45 d periodic-  
 82 ity, but no additional period was found.

## 83 4.2. Analysis of spectroscopic data

### 84 4.2.1. The spectrum at minimum

85 The spectrum taken at minimum shows emission in  $H\alpha$  and  $\text{He I } \lambda\lambda 5875\text{\AA}$   
 86 and  $\text{He I } \lambda\lambda 6678\text{\AA}$  in absorption, revealing an early type, possibly B-type  
 87 stellar component (Fig. 5). The Paschen series is seen in absorption, along  
 88 with double emission showing the violet peak larger than the red peak, i.e.  
 89  $V > R$ , where  $V$  and  $R$  refers to the respective peak intensities. We also find  
 90  $\text{OI } \lambda\lambda 8446\text{\AA}$  as single emission and some metallic double emissions. The  
 91 spectrum shows a second Balmer discontinuity. This fact, along with the  
 92 presence of  $\text{HI}$  emission and sharp absorptions of elements  $\text{Cr II}$ ,  $\text{Ti I}$ ,  $\text{Ti II}$ ,  
 93  $\text{Fe I}$  and  $\text{Fe II}$  reveals the presence of a circumstellar envelope.

94 The stellar parameters of the stars were obtained from direct measure-  
 95 ments of the Balmer discontinuity. To this aim we used the BCD method  
 96 [4, 5] that has the advantage of studying the Balmer jump to recognize B-type  
 97 stars with circumstellar envelopes due to the presence of a second component  
 98 of the Balmer discontinuity [6, 23, 3, 2]. A strong second Balmer disconti-  
 99 nuity is present in the spectrum taken at the minimum intensity of the light  
 100 curve ( $m_v = 17.2$ ). Based on the height of the Balmer jump  $D_\star = 0.17$  and  
 101 its spectral position  $\lambda_1 = 41 \text{\AA}$ , we determined a spectral type B2/3 and  
 102 temperature  $T_{eff} = 19\,000 \text{ K}$  using the recent BCD calibration by Shokry et  
 103 al. [17]. A spectral type B2/3IV is consistent with  $V = 17.2$  in the SMC,  
 104 as reveal the study of the star SMC\_SC4 22859 with  $V = 17.1$  [15]. These

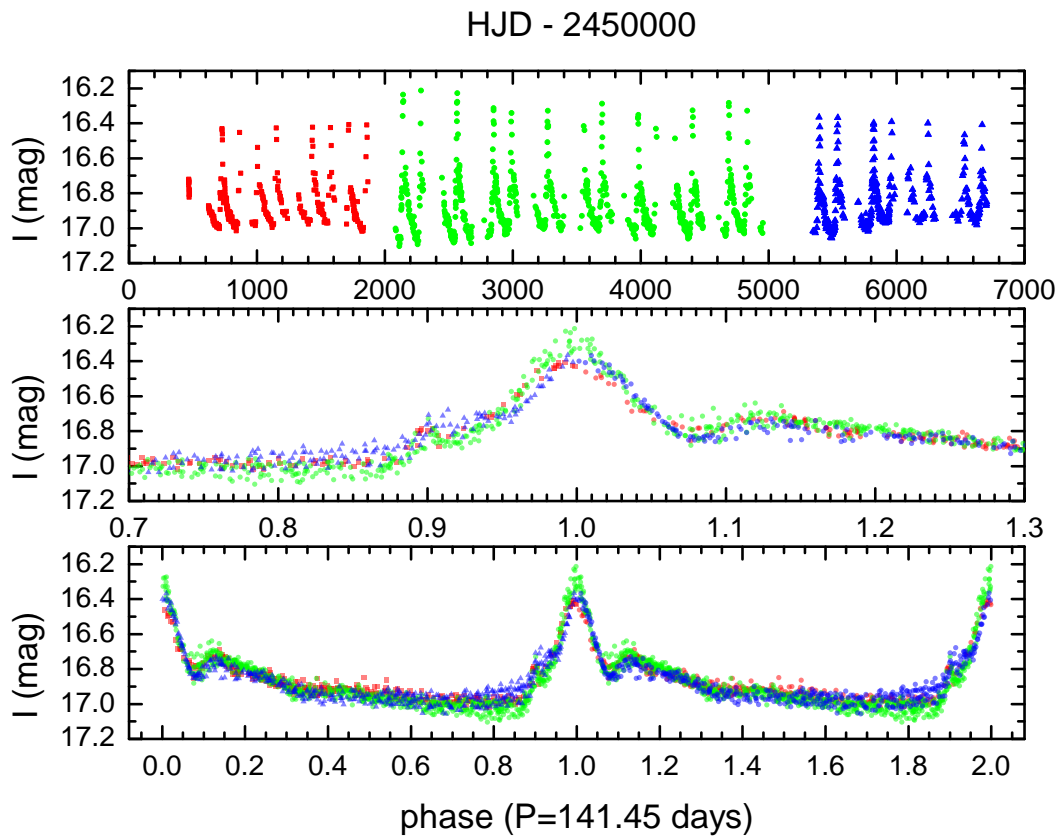


Figure 2: Fig. 1: OGLE *I*-band light curve (top panel), phased with the particular period (141.45 days: middle and bottom panels). Colors red, green and blue indicate magnitudes from photometric databases OGLE II, III and IV, respectively.

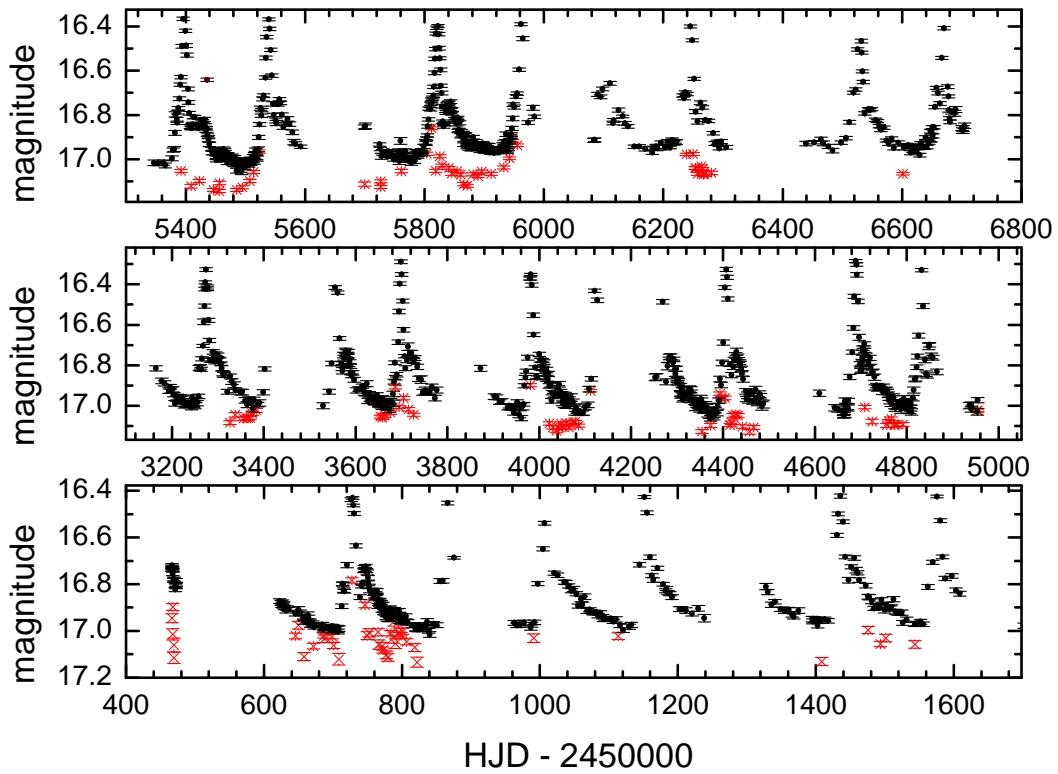


Figure 3: OGLE *I*-band (black dots) and *V*-band (red crosses) light curves at different epochs. Note the smaller amplitude variability in *V* band.



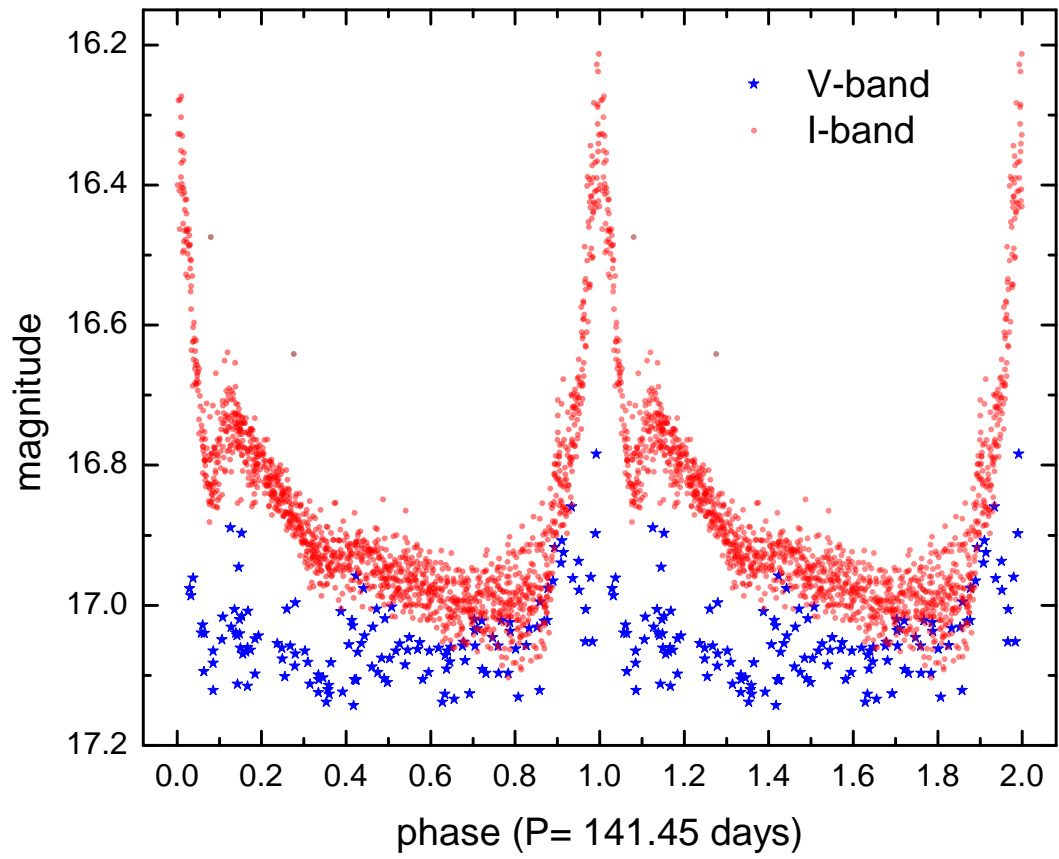


Figure 4: Comparison of *I*-band and *V*-band light curves during the 141.45 days cycle.

105 authors found 8 solar masses in the middle of the MS for SMC\_SC4 22859,  
106 and from our BCD analysis we get about 6.3 masses for our object, which is  
107 a reasonable discrepancy.

108 We also notice the similarity of the spectrum at minimum with the Galac-  
109 tic Be shell-star 48 Lib (HD 142983), classified as B8 Ia/Iab in SIMBAD. The  
110 comparison with the metallic absorption lines of 48 Lib produced in its en-  
111 velope is specially interesting; the comparison spectrum is taken from the  
112 UVES-POP catalogue<sup>6</sup> (Fig. 6). In the case of 48 Lib, this late classification  
113 is purely due to the shell, the actual star has a temperature corresponding to  
114 about B3 [18]. The supergiant classification is also only because of the shell,  
115 because it has a very strong V/R cycle (relative intensity between emission  
116 peaks) that can look like a P Cyg wind profile at times [18]. Some Fe II  
117 double emission lines with  $V > R$  are shown in Fig. 7 for comparison with  
118 the 48 Lib case.

#### 119 4.2.2. *The spectrum at maximum*

120 We observe much weaker Balmer absorptions than in minimum and He I  $\lambda\lambda 5875$   
121  $\text{\AA}$  appears as double emission with peak separation of  $240 \text{ km s}^{-1}$  (Fig. 8).  
122 As the spectrum is quite noisy in that region, and other helium lines as  
123 He I  $\lambda\lambda 4471 \text{ \AA}$  do not show emission, this detection should be considered  
124 as tentative only. Interestingly, as shown in Fig. 5, double emission is de-  
125 tected with confidence in the infrared Calcium triplet. At this stage the  
126 Balmer/Paschen double emissions are in general larger and without the deep  
127 absorption cores observed during minimum. The circumstellar metallic ab-  
128 sorption lines still are visible during maximum. An additional set of metallic  
129 lines appears, which are not observed at minimum, this is specially evident in  
130 the blue spectral region. Since they span the whole spectrum in the spatial  
131 direction at both sides of the stellar profile, this background metallic line  
132 spectrum probably arises from reflected moon light. In spite of this contam-  
133 ination, a set of lines characterized by radial velocities displaced by about  
134  $+140 \text{ km/s}$  from the background spectrum are present. Their velocities are  
135 compatible with an origin in the SMC and we assumed they are formed in  
136 the system under study.

137 At maximum we also find a stronger stellar NaD doublet (Fig. 8). The  
138 system NaD lines are clearly distinguished from the sharp Galactic interstel-

---

<sup>6</sup><http://www.eso.org/sci/observing/tools/uvespop.html>

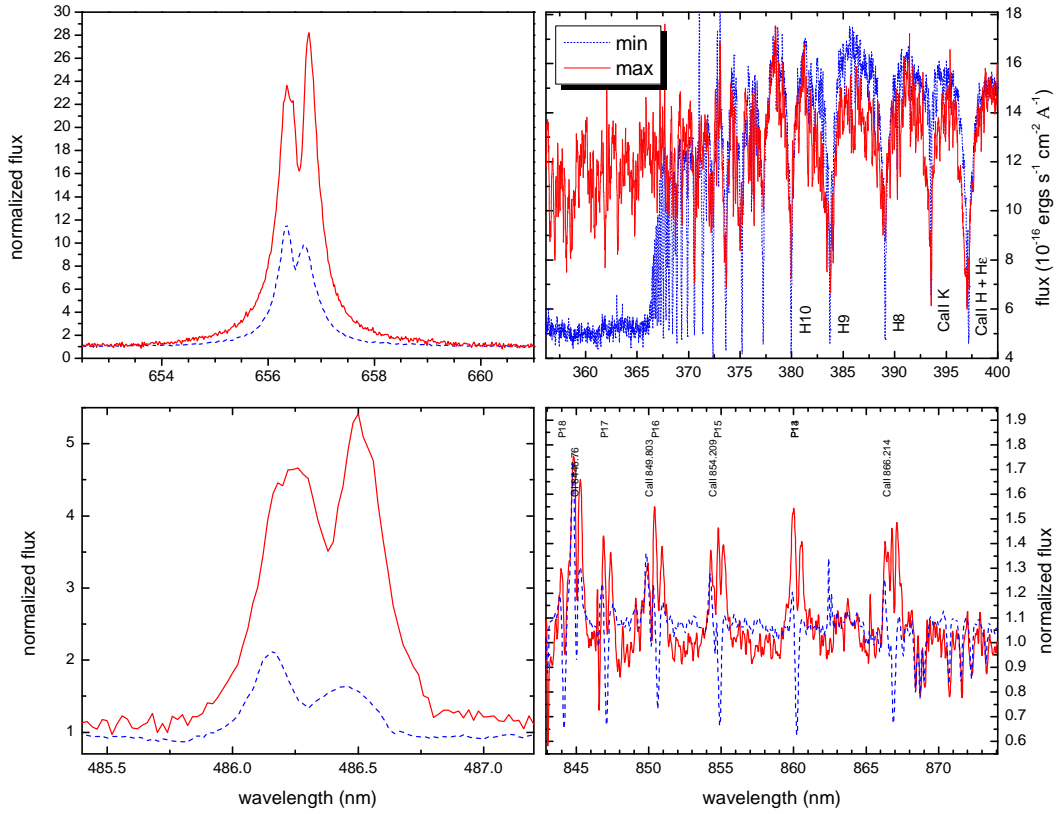


Figure 5: Comparison of spectral regions at maximum (solid red line) and minimum (dashed blue line). The flux calibration of the spectrum at maximum should not be trusted because of the contamination discussed in the text.

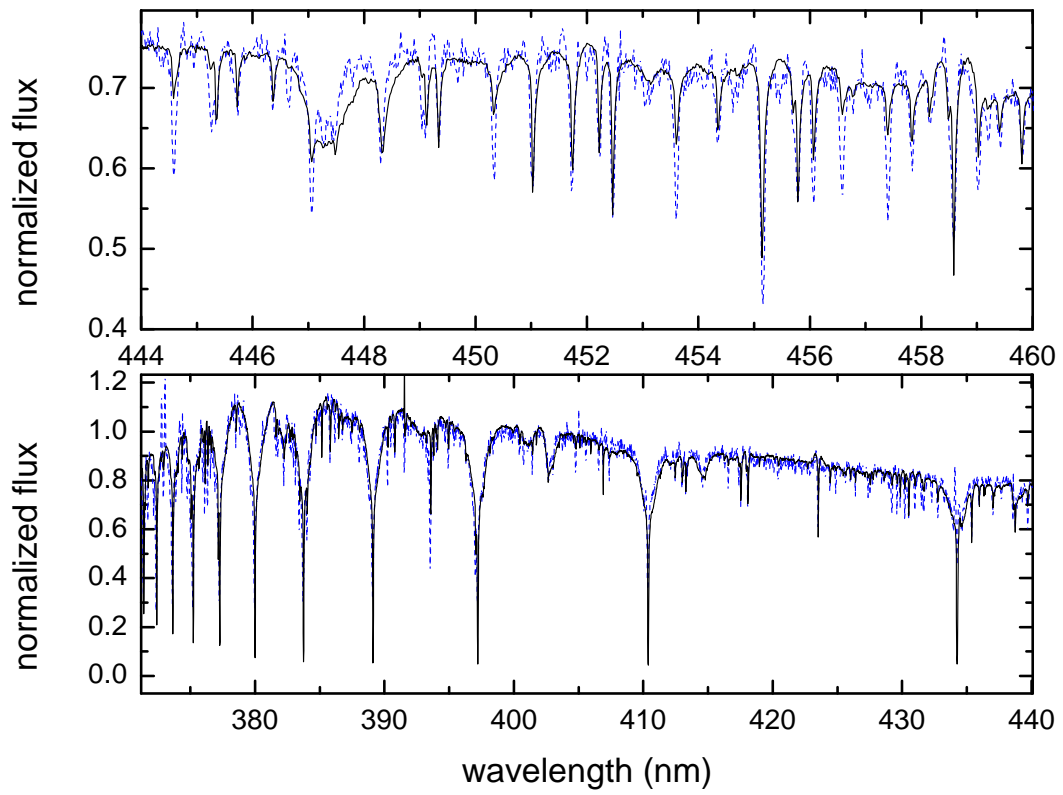


Figure 6: Comparison of the spectrum at minimum (dashed blue line) with the spectrum of 48 Lib (HD 142983) which is classified B8 Ia/Iab.

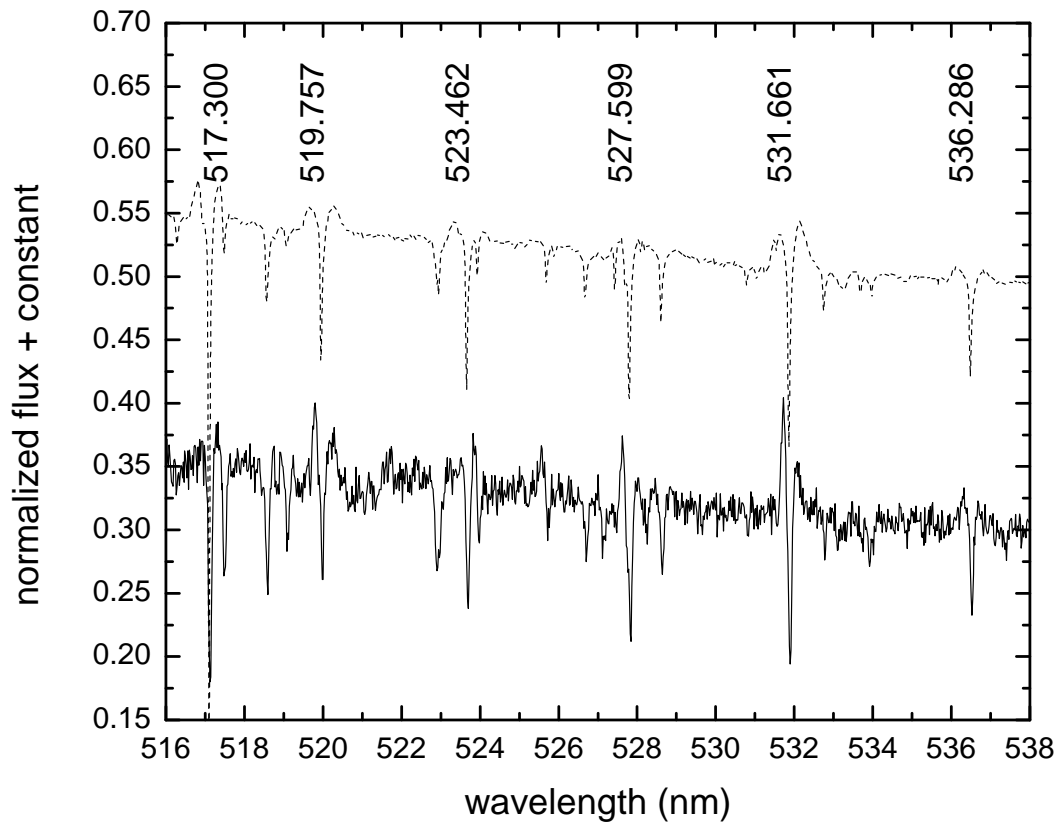


Figure 7: Some FeII double emission lines mostly showing the asymmetry  $V > R$  (solid-line) and the comparison with the 48 Lib spectrum (dashed-line).

139 lar NaD lines, that are more clearly visible at minimum. The SMC inter-  
 140 stellar components are expected much weaker than the Galactic ones and  
 141 are obviously masked by the system components, which are much stronger  
 142 than expect for a B-type star, and are probably formed in the circumstellar  
 143 medium. The increasing strength at maximum, along with the infrared Ca II  
 144 triplet emission suggest an accretion phenomenon and a formation in a mass  
 145 stream as we will discuss in Section 5.

#### 146 *4.2.3. General spectroscopic analysis*

147 Average properties for Balmer and Paschen emission lines are presented in  
 148 Table 3, including the ratio between the violet and red peak intensity relative  
 149 to the normalized continuum  $V/R \equiv (I_V - 1)/(I_R - 1)$ . The peak separation  
 150 increases with the Balmer series order. This gradient, and the existence of  
 151 double emission, are typical signatures of a Keplerian Be star disk. Equiva-  
 152 lent widths ( $EW$ ) were measured between the adjacent continuum of the  $H\alpha$   
 153 line and tracing a line at the base of the other emission lines.

154 In general we notice larger H I emission at maximum, along with changes  
 155 in H I line shapes. At minimum  $V > R$  and at maximum  $V < R$  in Balmer  
 156 lines. However, in Paschen lines  $V > R$  in both epochs. At maximum, we  
 157 also observe Ca II lines as double emissions. While the  $H\alpha$  peak separation  
 158 increases at maximum the opposite is observed in  $H\beta$ .  $H\beta$  remains almost of  
 159 the same strength relative to the continuum at both epochs.

160 Radial velocities for He I, Si I and NaD absorption lines are given in Table  
 161 4, for Fe II emission lines (along with peak separation) are given in Table 5  
 162 and for H I and metallic absorption lines are given in Table 6. At maximum  
 163 we observe a bimodal distribution of the radial velocities suggesting two  
 164 components, and at minimum only one component is clearly observed (Fig.  
 165 9); this fact suggests furthermore that the system is a binary star.

## 166 **5. Discussion**

167 At minimum the B-type component dominates the spectrum and the set  
 168 of radial velocities of the envelope roughly matches those helium-line veloci-  
 169 ties associated to the star (Table 4 and 6). This suggests that a circumstellar  
 170 envelope surrounds the B-type star. The double peak structure of the H I  
 171 emission and the presence of V/R variability suggests a disc-shaped envelope.  
 172 V/R variability is usually observed in Be stars and interpreted as oscillations  
 173 of density enhancements and explained by the one-armed oscillation theory

Table 3: Average measurements for emission lines and their standard deviations. The methods of barycenter and central minimum are indicated for radial velocities with typical error  $\pm 2$  km/s.

Line	$EW$ ( $\text{\AA}$ )	$\Delta\lambda_p$ ( $\text{km s}^{-1}$ )	$V/R$ or note	RV(bar) ( $\text{km s}^{-1}$ )	RV(cen) ( $\text{km s}^{-1}$ )
min					
H $\alpha$	$-102.8 \pm 0.5$	$153 \pm 3$	$1.19 \pm 0.01$	103	107
H $\beta$	$-5.0 \pm 0.1$	$186 \pm 6$	$1.76 \pm 0.01$	82	101
H $\gamma$	NA	$225 \pm 2$	$V > R$	90	120
P14	$0.50 \pm 0.05$	-	-	-	132
P17	-	-	-	-	132
max					
H $\alpha$	$-269.7 \pm 3.0$	$179 \pm 2$	$0.83 \pm 0.04$	142	139
H $\beta$	$-24.0 \pm 0.2$	$159 \pm 1$	$0.83 \pm 0.02$	158	156
H $\gamma$	$-3.9 \pm 0.2$	$188 \pm 5$	$V \sim R$	164	154
P14	$-4.7 \pm 0.5$	$198 \pm 5$	$1.33 \pm 0.01$	135	148
P17	$-5.0 \pm 0.5$	$205 \pm 5$	$1.20 \pm 0.01$	144	149
He I 5875	$-1.0 \pm 0.5$	$240 \pm 5$	$V \sim R$	219	180

Table 4: Radial velocities of some absorption lines at maximum and minimum.

Line	RV ( $\text{km s}^{-1}$ )
min	
He I 5875	$109 \pm 15^*$
Si I 6347.1	$123.8 \pm 0.2$
He I 6678	$127 \pm 3$
Na I 5889.95	$122.7 \pm 0.2$
Na I 5895.92	$125.2 \pm 0.2$
Mean (min)	$125 \pm 2$
excluding *	
max	
Na I 5889.95	$145.8 \pm 0.2$
Na I 5895.92	$147.7 \pm 0.2$
Si I 6347.1	$147.0 \pm 0.2$
Mean (max)	$147 \pm 1$

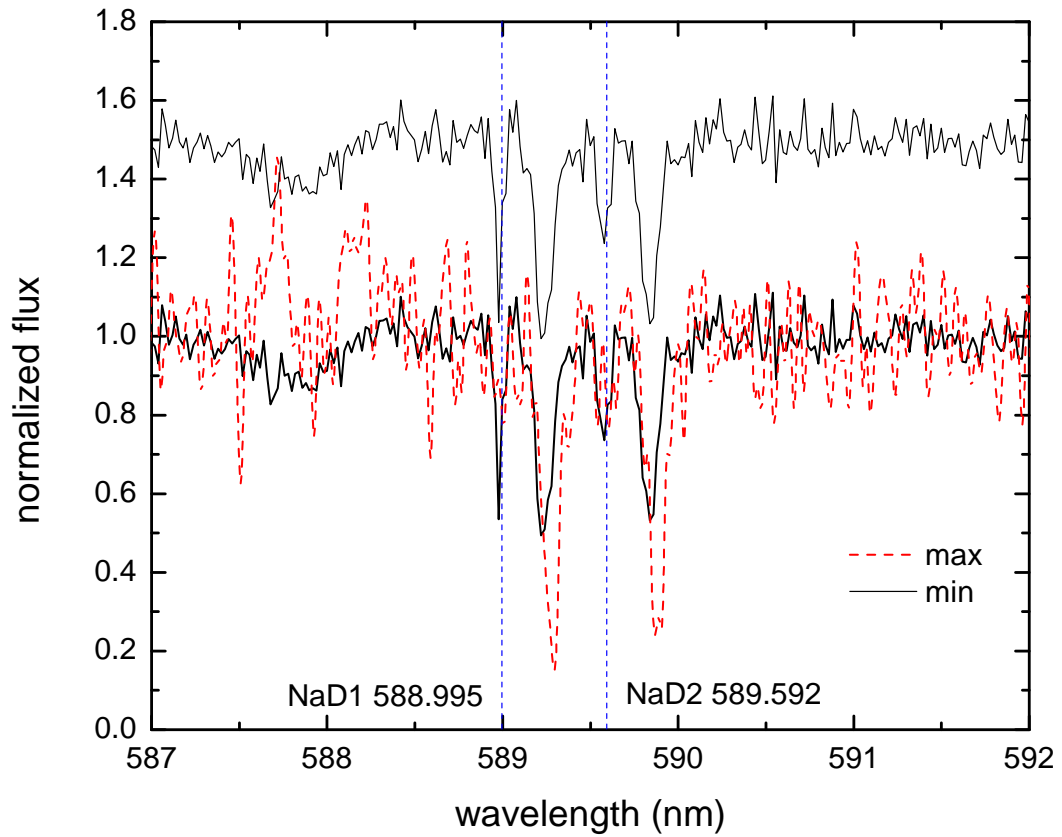


Figure 8: NaD and He I 5875 lines at maximum (dashed red line) and minimum (black). Vertical dashed lines indicate rest wavelengths for D1 and D2 lines of Na. The absorption lines at the rest wavelengths are due to Galactic interstellar absorption. The spectrum at minimum is plotted twice and shifted for easier comparison.



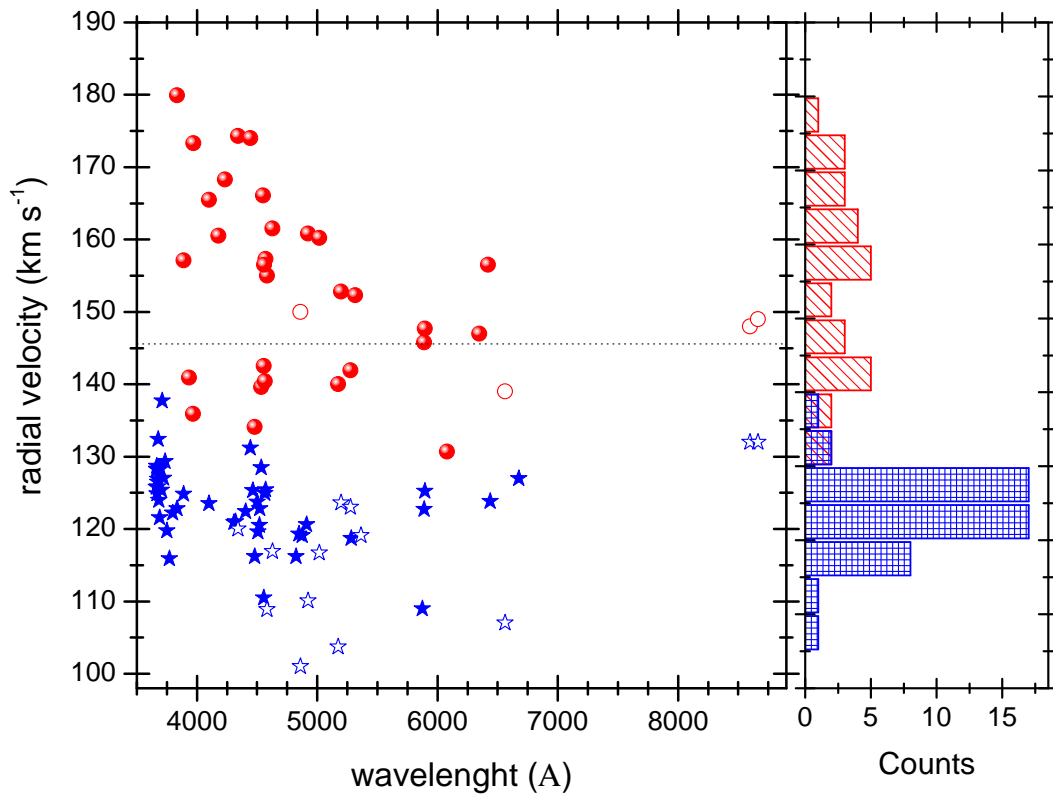


Figure 9: Radial velocities of absorption lines at maximum (red spheres) and minimum (blue stars) and the respective histograms. Open symbols indicating central absorption radial velocity of double emission lines are also shown. The heliocentric velocity of the SMC,  $145.6 \text{ km s}^{-1}$  [10] is indicated as a dotted line.

Table 5: Radial velocities and peak separation for double-emission FeII lines observed during minimum.

$\lambda$ (lab) ( $\text{\AA}$ )	abs ( $\text{km s}^{-1}$ )	blue-em ( $\text{km s}^{-1}$ )	red-em ( $\text{km s}^{-1}$ )	$\Delta\lambda_p$ ( $\text{km s}^{-1}$ )
4233.167	118.9	16.2	222.3	206.1
4583.829	108.9	-0.4	241.0	241.3
4629.336	116.9	20.4	234.8	214.4
4924.043	110.1	4.1	–	–
5018.434	116.7	11.0	213.5	202.5
5173.002	103.7	-8.1	–	–
5197.569	123.6	10.5	257.4	246.9
5275.994	123.0	-0.9	–	–
5316.609/777	118.6	17.1	209.4	192.3
5362.864	119.1	4.5	–	–
Average	115.9	7.5	229.7	217.2
std	6.4	9.2	18.2	22.0

174 [13]. Furthermore, quasi-cyclic photometric variability in time scales of thou-  
175 sands of days, as observed in this system, has been sometimes reported in Be  
176 stars. We notice that the observed long-cycle period of 2500 days (6.8 years)  
177 is close to the average of the V/R variability time-scale, viz. 7 years [12].  
178 The above suggests a Be star nature for this system. The Classical Be stars  
179 are rapidly rotating non-supergiants B-type stars that show or have shown  
180 Balmer line emission in the past [16]. The emission is formed in a circumstel-  
181 lar disk by electron excitation and subsequent cascade recombination in the  
182 circumstellar material, mostly neutral hydrogen. On the observational side,  
183 the system show similarities to the Be star ABE-A01, showing outbursts with  
184 a quasi-period of 91.23 days [8].

185 At maximum we observe two sets of radial velocities clearly separated and  
186 different from the radial velocities observed at minimum. This fact, along  
187 with the shape of the light curve, might indicate that the system is a binary  
188 of orbital period 141.45 days with a dense circumstellar disc and an eccentric  
189 orbit. Furthermore, we notice that at maximum the  $H\alpha$  and Paschen emission  
190 are larger and the NaD lines are stronger, indicating possibly a mass transfer  
191 episode in an eccentric binary system when the unseen secondary star passes  
192 at periastron, overflowing its Roche lobe and depositing material onto the

193 Be star disc. Supporting this accretion scenario, the detection of the infrared  
194 Ca II triplet in emission in Be stars has been interpreted in terms of binarity  
195 and stream accretion [7, 17]. However, at the present stage, we cannot discard  
196 the possibility that during periastron passage an increased injection of mass  
197 might occur from the surface of the Be star into the disk, producing the  
198 observed brightenings (ejection scenario).

199 Future challenges include the determination of the nature of the unseen  
200 secondary star and the determination of the orbital parameters, including an  
201 explanation for the possible eccentricity. The secondary is probably not a  
202 compact object, because of the lack of X-ray and high-excitation lines, and  
203 also because the outbursts are of low amplitude, reflecting - in the accretion  
204 scenario - the fall of material into a shallow gravitational potential. On the  
205 other hand, the secondary star should be much less luminous than the Be  
206 star to remain undetected in the spectrum. This suggests a lower tempera-  
207 ture main-sequence secondary star. In the ejection scenario, its mass should  
208 be not so low in order to perturb appreciably the gravitationally bounded  
209 material in the surface of the Be star. Another possibility is a low-mass OB  
210 subdwarf secondary, as seen in HR 2142 [14] and other recently found Be +  
211 sdO Galactic binaries [22]. These relatively hot but very faint objects were  
212 detected only in combined spectra with very high signal to noise obtained  
213 in the ultraviolet spectral region by the *International Ultraviolet Explorer*  
214 satellite.

## 215 6. Conclusions

216 Based on the study of 17.5 years of *I*- and *V*-band OGLE photometry and  
217 new X-SHOOTER spectra we find that OGLEJ005039.05-725751.4 is very  
218 likely a binary consisting of a Be star in an eccentric orbit with orbital period  
219 141.45 days. We also detect a long-cycle of 2500 days in the photometric  
220 dataset. The strange character of the light curve might be explained by  
221 periodic mass transfer in a complex binary system as happens in certain types  
222 of cataclysmic variables. This is supported by our finding that at maximum  
223 the H $\alpha$  emission is larger, the infrared Calcium triplet is seen in emission and  
224 the NaD lines are stronger. A detailed explanation of the system is beyond  
225 the capabilities of the available data. Future plans include the acquisition  
226 of time resolved spectroscopy to resolve the binary orbit and enlighten the  
227 brightening and line emission enhancement episode.

Table 6: Radial velocities of absorption lines observed during minimum. The observed wavelengths are not barycentric corrected (the velocities do).

$\lambda$ (lab) ( $\text{\AA}$ )	$\lambda$ (obs) ( $\text{\AA}$ )	RV ( $\text{km s}^{-1}$ )
H I		
3663.406	3664.943	125.8
3664.679	3666.252	128.7
3666.097	3667.666	128.3
3667.684	3669.212	124.9
3669.466	3671.035	128.2
3671.478	3673.019	125.8
3673.761	3675.316	126.9
3676.365	3677.916	126.5
3679.355	3680.980	132.4
3682.810	3684.333	124.0
3686.833	3688.414	128.6
3691.557	3693.054	121.6
3697.154	3698.736	128.3
3703.855	3705.404	125.4
3711.973	3713.678	137.7
3721.940	3723.517	127.0
3734.370	3735.981	129.3
3750.154	3751.652	119.8
3770.632	3772.090	115.9
3797.900	3799.448	122.2
3835.386	3836.957	122.8
3889.051	3890.670	124.8
4101.737	4103.427	123.5
Fe I		
4307.902	4309.796	120.9
4404.750	4406.709	122.4
Fe II		
4508.288	4510.250	119.6
4520.224	4522.205	120.5
4522.634	4524.651	122.8
4555.893	4557.738	110.5
4848.235	4850.341	119.3
5284.109	5286.394	118.7
Ti II		
4320.960	4322.861	121.0
4443.798	4445.904	131.2
4464.450	4466.479	125.3
4501.272	4503.293	123.7
4533.966	4536.075	128.5
4911.193	4913.348	120.6
4563.761	4565.828	124.9
4571.969	4574.048	125.4
Mg II		
4481.226	4483.126	116.2
Cr II		
4824.127	4826.172	116.2
4876.440	4878.554	119.1
Average $\pm$ std	-	123.9 $\pm$ 5.0

Table 7: Radial velocities of absorption lines observed during maximum.

$\lambda$ (lab) ( $\text{\AA}$ )	$\lambda$ (obs) ( $\text{\AA}$ )	RV ( $\text{km s}^{-1}$ )
H		
4340.472	4342.93	174.3
4101.737	4103.94	165.5
3970.075	3972.31	173.3
3889.051	3891.03	157.1
3835.386	3837.63	179.9
Fe II		
4178.855	4181.03	160.5
4233.167	4235.48	168.3
4549.467	4551.92	166.1
4555.893	4557.99	142.5
4583.829	4586.13	155.0
4629.336	4631.76	161.5
4924.043	4926.61	160.8
5018.434	5021.04	160.2
5173.002	5175.34	140.0
5197.569	5200.14	152.8
5275.994	5278.41	141.9
5316.609	5319.23	152.3
Ca II		
3933.660	3935.45	140.9
3968.470	3970.21	135.9
Mg II		
4481.226	4483.17	134.1
Ti II		
4443.798	4446.31	174.0
4533.966	4536.01	139.6
4563.761	4565.83	140.4
4571.969	4574.3	157.3
Cr II		
4558.659	4560.97	156.5
Fe I		
6078.500	6081.06	130.7
6419.980	6717.13	156.5
Average	-	$154.0 \pm 13.0$

## 228 **7. Acknowledgments**

229 Thanks to the anonymous referee for providing useful comments that im-  
230 proved the first version of this manuscript. This research has made use of the  
231 SIMBAD database, operated at CDS, Strasbourg, France. R.E.M. acknowl-  
232 edges support by VRID-Enlace 218.016.004-1.0, VRID-Enlace 216.016.002-  
233 1.0 and the BASAL Centro de Astrofísica y Tecnologías Afines (CATA) PFB-  
234 06/2007. LC acknowledges financial support from the Agencia de Promoción  
235 Científica y Tecnológica (Préstamo BID PICT 2016/1971), CONICET (PIP  
236 0177), and the Universidad Nacional de La Plata (Programa de Incentivos  
237 G11/137), Argentina. L.C. thanks also support from the project CONI-  
238 CYT + PAI/Atracción de capital humano avanzado del extranjero (folio  
239 PAI80160057). The OGLE project has received funding from the Polish Na-  
240 tional Science Centre grant MAESTRO no. 2014/14/A/ST9/00121.

## 241 **References**

- 242 [1] Abt H. A., Levato H., Grosso M., 2002, *ApJ*, 573, 359
- 243 [2] Aidelman Y., Cidale L. S., Zorec J., Panei J. A., 2018, *A&A*, 610, A30
- 244 [3] Aidelman Y., Cidale L. S., Zorec J., Panei J. A., 2015, *A&A*, 577, A45
- 245 [4] Barbier D., Chalonge D., 1939, *ApJ*, 90, 627
- 246 [5] Chalonge D., Divan L., 1973, *A&A*, 23, 69
- 247 [6] Divan L., 1979, *RA*, 9, 247
- 248 [7] Koubský P., et al., 2012, arXiv, arXiv:1205.2259
- 249 [8] Labadie-Bartz J., et al., 2018, *AJ*, 155, 53
- 250 [9] Martayan C., Baade D., Fabregat J., 2010, *A&A*, 509, A11
- 251 [10] McConnachie A. W., 2012, *AJ*, 144, 4
- 252 [11] Mennickent R. E., Pietrzyński G., Gieren W., Szewczyk O., 2002, *A&A*,  
253 393, 887
- 254 [12] Mennickent R. E., Vogt N., 1991, *A&A*, 241, 159

- 255 [13] Okazaki A. T., 1991, PASJ, 43, 75
- 256 [14] Peters G. J., Wang L., Gies D. R., Grundstrom E. D., 2016, ApJ, 828,  
257 47
- 258 [15] Rímulo L. R., et al., 2018, MNRAS, 476, 3555
- 259 [16] Rivinius T., Carciofi A. C., Martayan C., 2013, A&ARv, 21, 69
- 260 [17] Shokry A., et al., 2018, A&A, 609, A108
- 261 [18] Silaj J., et al., 2016, ApJ, 826, 81
- 262 [19] Stellingwerf R. F., 1978, ApJ, 224, 953
- 263 [20] Szymanski M. K. 2005, AcA, 55, 43
- 264 [21] Udalski A., Szymański M. K. & Szymański G. 2015, AcA, 65, 1
- 265 [22] Wang L., Gies D. R., Peters G. J., 2018, ApJ, 853, 156
- 266 [23] Zorec J., Briot D., 1991, A&A, 245, 150